How Social Attributes Affect the Movement Process of Subgroups When Facing a Static Obstacle

Wenhan Wu, Wenfeng Yi, Erhui Wang, Xiaolu Wang, and Xiaoping Zheng

***Abstract*—With the increasing number of studies on crowd behavior analysis, there has been a widespread interest in treating subgroups as an important topic. A previous experimental study has investigated the decision-making and motion behavior of subgroups when facing a static obstacle during movement. However, it is hard to quantify social attributes (e.g., interpersonal relationships and sense of identity) and little is known about how they affect the movement process of subgroups. Here, we propose a vision-driven model to solve this problem, in which two key model parameters are defined to control the spatial cohesion and attraction intensity, respectively. Numerical simulations demonstrate that the optimal regions of model parameters vary depending on different conditions of the three control variables (obstacle width, time pressure, and subgroup size). The spatial cohesion and attraction intensity barely change the movement process of subgroups in the maintaining state but significantly affect it in the splitting-merging state. This model can reproduce the herding effect of subgroup members in the merging process, which is affected to varying degrees by the modulation of model parameters. Overall, this work contributes to the simulation of subgroup behaviors from a sociopsychological perspective.**

***Index Terms*—Cognitive heuristics, modeling and simulations, social attributes, static obstacle, subgroup behaviors.**

I. Introduction

As human crowds exhibit diverse collective patterns in different contexts, crowd behavior analysis has become a key research field and attracted a wide range of interest [1], [2]. It includes many aspects such as trajectory prediction [3], scene segmentation [4], crowd counting [5], behavior recognition [6], and anomaly detection [7], covering various behavioral characteristics of human crowds in temporal and spatial dimensions. Understanding the laws and dynamics of crowd behavior can provide important decision support for urban planning, emergency management, public safety, and other applications [8], [9], which helps to improve the overall efficiency of social systems and promote the construction of smart cities. In most studies, however, it is assumed for simplicity that human crowds are composed of isolated individuals, but this is inconsistent with the ubiquity of subgroups (i.e., a collective term for "social groups," "pedestrian groups," and "small groups" in other literature) [10]. In the context of crowd behavior analysis, subgroups refer to relatively independent clusters or subsets in human crowds, who are geographically close and attempt to move in a congregated form [11]. Given the crucial role that subgroups play in linking the individual and group levels of observation, a growing body of research has recognized the importance of considering subgroups as a specific topic in recent years.

According to research methods, existing studies related to subgroups are basically divided following three directions. In terms of field observations, the number of subgroups has been confirmed to decrease with the growing size, and it follows a zero-truncated Poisson distribution [12]. The spatial configuration of subgroups was observed to present a horizontal formation at low density, a "V"-like or "U"-like structure at moderate density, and a "river"-like pattern at extremely high density [8], [13]. The walking speed of subgroups was also found to decrease as the size increases under normal conditions [14]. With regard to controlled experiments, how the presence of subgroups changes the speed- and flow-density relations in fundamental diagrams was often explored in uni- and bidirectional corridors [15], [16]. The effects of subgroup size, cooperative behavior, decision making, and other factors on evacuation processes were the focus in single- and multiple-exit rooms [17], [18]. Besides, virtual reality technology was also used in emergency scenarios to investigate the social interactions of subgroup members and validate observed phenomena and model performance [19], [20]. Regarding modeling and simulations, subgroup models have mainly been improved based on three mainstream models (i.e., social force model [21], cellular automata model [22], and agent-based model [23]) by incorporating elements such as the leader–follower principle [24], cohesion effect [25], and behavioral rules [26], which aims to study the impacts of subgroups on traffic dynamics and crowd evacuation [12], [27]. Nonetheless, it is found that these studies seldom focus on the behavioral characteristics of subgroups when facing obstacles, but obstacles have always been essential to individual interactions in crowd dynamics [28], [29].

To fill the lack of research in this aspect, we previously conducted an experimental study to investigate the decision-making and motion behavior of subgroups when facing a static obstacle [30]. Specifically, a retractable static obstacle was

Received 13 May 2024; revised 21 September 2024; accepted 5 November 2024. This work was supported in part by the National Key Research and Development Program of China under Grant 2021YFB3301100 and in part by the National Major Scientific Research Instrument Development Project under Grant 61927804. *(Corresponding author: Xiaoping Zheng.)*

The authors are with the Department of Automation, Beijing National Research Center for Information Science and Technology, Tsinghua University, Beijing 100084, China (e-mail: wwh19@mails.tsinghua.edu.cn; yiwf22@mails.tsinghua.edu.cn; erhuiwang@mail.tsinghua.edu.cn; wangxlu@mail.tsinghua.edu.cn; asean@mail.tsinghua.edu.cn).

Digital Object Identifier 10.1109/TCSS.2024.3493954

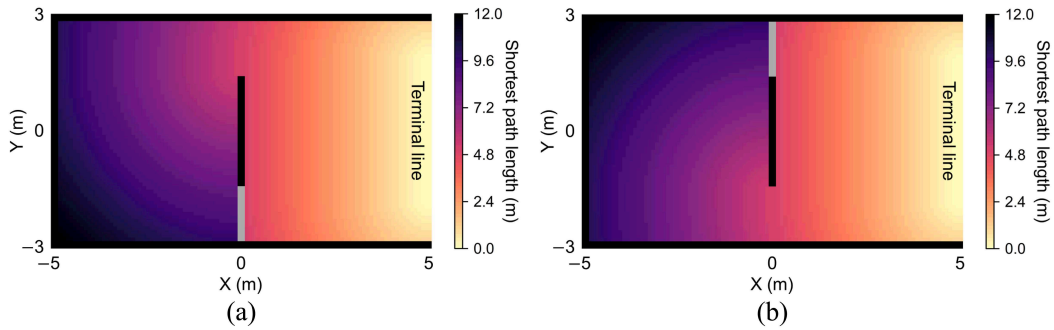

Fig. 1. Shortest path length from each position point to the terminal line in the experimental scenario. (a) Right-side passable area of the obstacle is blocked. (b) Left-side passable area of the obstacle is blocked.

placed in the middle of a rectangular scenario, and randomly composed subgroups were asked to move from the initial area to the terminal line within a certain time. We then combined different values of the three control variables: obstacle width (2, 3, 4 m), time pressure ($+\infty$, 8, 5 s), subgroup size (2, 3, 4), and performed 12 replicated rounds for each of the 27 experimental conditions. Based on the extracted data, the movement states and preferences of subgroups during movement, the differences in path length, movement time, and average speed between the maintaining and splitting-merging states, as well as the changes in various physical quantities in the splitting and merging processes were analyzed in detail. However, given that all subgroups in experiments were randomly composed of participants following certain assignments, a core issue in our previous study is the difficulty in quantifying social attributes (e.g., interpersonal relationships and sense of identity) and exploring how they affect the movement process of subgroups when facing a static obstacle. This is because different social attributes can determine the interaction behavior among members [31], [32], which may be manifested as the differences in spatial cohesion and attraction intensity of subgroups in our case.

Therefore, we develop a vision-driven model to address this issue. The mathematical description of subgroup decision-making is given and consistent with the results under experimental conditions. The cognitive heuristics for subgroup movement are defined based on the perception of visual information, and relevant findings of subgroup motion behavior in experiments are integrated into this model. Two key model parameters $d_i^{\min}$ and $d_i^{\max}$ are the minimum and maximum critical distances that determine how the follow willingness coefficient α_i varies, which can be used to control the spatial cohesion and attraction intensity, respectively. By conducting numerical simulations, how the three control variables affect the optimal regions of model parameters is first investigated. Then, the effects of spatial cohesion and attraction intensity on the movement process are further analyzed. Last, we validate the ability of this model to reproduce the herding effect in the merging process and discuss the influence of model parameters on it. Our results indicate that social attributes are clearly an indispensable factor that mainly exerts a significant effect on subgroup movement in the splitting-merging state, which is important for better understanding subgroup behaviors.

The rest of this article is organized as follows. In Section II, a vision-driven model is proposed with parameter settings. Section III conducts numerical simulations to analyze the effects of model parameters and validate the reproducibility of this model. Finally, relevant conclusions and future prospects are summarized in Section IV.

II. Model

A. Mathematical Description of Subgroup Decision-Making

The previous study has theoretically analyzed the movement states and preferences of subgroups when facing a static obstacle [30], which can be transformed into mathematical representations here. On the one hand, the movement state X_g of subgroup g is divided into two types: the maintaining state ($X_g = 0$) represents that members pass through the obstacle in a congregated form and arrive at the terminal line together, and the splitting-merging state ($X_g = 1$) means that members first split to pass through the obstacle and then merge to reach the terminal line. On the other hand, the movement preference Y_g of subgroup g is divided into three types: the left-side preference ($Y_g = -1$) indicates that more members pass from the left side of the obstacle, and vice versa for the right-side preference ($Y_g = 1$), while the equal-side preference ($Y_g = 0$) denotes that the number of members passing from both sides is the same. Given that movement preferences are formed on the basis of movement states, the probability that subgroup g makes a specific decision is defined as $P(Y_g = n \,|X_g = m)$, where $m = \{0, 1\}$ and $n = \{-1, 0, 1\}$.

The decision-making on movement states and preferences is manifested in the behavior of each member in the initial area choosing which side of the obstacle to pass through, and this will determine the direction of the shortest path toward the terminal line. From this, we assume that the right-side passable area is blocked when an individual chooses to pass from the left side of the obstacle, and vice versa, the left-side passable area will be blocked. For these two kinds of decisions to pass through the obstacle, as shown in Fig. 1, the shortest path $d(\mathbf{x})$ from each position point $\mathbf{x}$ to the terminal line in the experimental scenario is approximately calculated by a 2-D Eikonal equation $\|\nabla d(\mathbf{x})\| = 1$, and its negative gradient $-\nabla d(\mathbf{x})$ corresponds to the direction of the shortest path toward the terminal line.

Note that this direction is not the desired direction of individuals during movement.

B. Cognitive Heuristics for Subgroup Movement

The cognitive heuristics for subgroup movement are related to the perception of visual information [33], reflected in the decision-making of subgroup member i when interacting with objects in its own visual projection field S_i^{vis} (i.e., a sector area with a maximum horizon distance $d_{\max}$, ranging to the left and to the right by φ degree with respect to the line of sight $\mathbf{h_i}$) [34]. The first heuristic "A subgroup member chooses a trade-off between the individual desired direction and the subgroup desired direction" determines the desired direction of subgroup member i, as given by

$$\mathbf{e}_i^{\text{des}} = \frac{(1-\alpha_i)\,\mathbf{e}_i^{\text{ind}} + \alpha_i \mathbf{e}_i^{\text{sub}}}{\left\|(1-\alpha_i)\,\mathbf{e}_i^{\text{ind}} + \alpha_i \mathbf{e}_i^{\text{sub}}\right\|}. \tag{1}$$

First, a subgroup member often chooses the most direct path to reach the destination point O_i in the presence of other individuals and obstacles, whereby the angle θ_i^{ind} corresponding to the individual desired direction $\mathbf{e}_i^{\text{ind}}$ can be obtained by minimizing a square function of the distance to the destination at directional angle $\theta \in [-\varphi, \varphi]$

$$d(\theta) = d_{\max}^2 + f(\theta)^2 - 2 d_{\max} f(\theta) \cos(\theta_0 - \theta) \tag{2}$$

where θ_0 is the directional angle of the destination point O_i, and $f(\theta)$ is the expected distance to the first collision if member i moves into directional angle θ at speed v_i^{avs}. To maintain a congregated form, a subgroup member also tends to be attracted by other members in the field of view until entering a certain local interaction range, which produces the expression of the subgroup desired direction $\mathbf{e}_i^{\text{sub}}$

$$\mathbf{e}_i^{\text{sub}} = \frac{\langle \mathbf{x}_q \rangle_{q \in S_i^{\text{vis}}} - \mathbf{x}_i}{\left\| \langle \mathbf{x}_q \rangle_{q \in S_i^{\text{vis}}} - \mathbf{x}_i \right\|} \tag{3}$$

where $\mathbf{x}_q$ are the positions of other members q within the visual projection field S_i^{vis}. It should be noted that for subgroups moving in a splitting-merging state, before passing through the obstacle, only those who satisfy the same decision-making as subgroup member i can be regarded as other members q (i.e., the attraction of other members on the other side is not taken into account in the splitting process). In addition, as a key weighting factor in (1), the follow willingness coefficient α_i is defined as follows:

$$\alpha_i = \begin{cases} 0, & d_{ic} < d_i^{\min} \\ \frac{d_{ic} - d_i^{\min}}{d_i^{\max} - d_i^{\min}}, & d_i^{\min} \le d_{ic} \le d_i^{\max} \\ 1, & d_{ic} > d_i^{\max} \end{cases} \tag{4}$$

where $d_{ic} = \left\| \langle \mathbf{x}_q \rangle_{q \in S_i^{\text{vis}}} - \mathbf{x}_i \right\|$ is the distance from subgroup member i to the centroid of other members within the visual projection field S_i^{vis}. $d_i^{\min}$ and $d_i^{\max}$ are the minimum and maximum critical distances, between which the follow willingness coefficient α_i varies linearly with d_{ic}.

The second heuristic "A subgroup member adjusts the desired speed in avoiding collisions with obstacles and avoiding separation from the subgroup" defines the desired speed of subgroup member i

$$v_i^{\text{des}} = \min\left(v_i^{\text{avc}}, v_i^{\text{avs}}\right). \tag{5}$$

On the one hand, a subgroup member should keep a safe distance from the nearest obstacle in the movement direction to ensure stopping within a time period τ_i before the collision occurs. As a consequence, the desired speed v_i^{avc} for avoiding collision is calculated as follows:

$$v_i^{\text{avc}} = \frac{d_i^h}{\tau_i} \tag{6}$$

where d_i^h is the distance to the first obstacle along the desired direction $\mathbf{e}_i^{\text{des}}$. On the other hand, the willingness to follow at a faster speed will become stronger if subgroup member i is farther away from the centroid of other members in the field of view. The expression of the desired speed v_i^{avs} for avoiding separation is given by

$$v_i^{\text{avs}} = (1-\alpha_i)\, v_i^0 + \alpha_i v_i^{\max} \tag{7}$$

where v_i^0 and $v_i^{\max}$ are the initial and maximum desired speeds of subgroup member i, respectively.

C. Equations of Motion for Subgroup Members

In mathematical form, the position $\mathbf{x}_i(t)$ of subgroup member i is updated by $d\mathbf{x}_i(t)/dt = \mathbf{v}_i(t)$, where the temporal variation of velocity $\mathbf{v}_i(t)$ is triggered by the following acceleration equation:

$$m_i \frac{d\mathbf{v}_i(t)}{dt} = \mathbf{f}_{id} + \sum_{j(\neq i)} \mathbf{f}_{ij} + \sum_W \mathbf{f}_{iW}. \tag{8}$$

Here, the first term $\mathbf{f}_{id}$ on the right side of the above equation describes a force that drives individuals to move toward the destination via the perception of visual information, which is expressed as follows:

$$\mathbf{f}_{id} = m_i \frac{v_i^{\text{des}}(t)\,\mathbf{e}_i^{\text{des}}(t) - \mathbf{v}_i(t)}{\tau_i} \tag{9}$$

where subgroup member i of mass m_i tends to move with a desired speed $v_i^{\text{des}}(t)$ in a desired direction $\mathbf{e}_i^{\text{des}}(t)$, and therefore adopts his or her actual velocity $\mathbf{v}_i(t)$ within a characteristic time τ_i. The second term $\mathbf{f}_{ij}$ represents a physical contact force caused by body collisions with other individuals at extreme densities

$$\mathbf{f}_{ij} = kg(r_{ij} - d_{ij})\,\mathbf{n}_{ij} \tag{10}$$

where k is a body elasticity coefficient, $\mathbf{n}_{ij}$ is the normalized vector pointing from individual j to i, r_{ij} and d_{ij} are the sum of their radii and the distance between their centers of mass. $g(x) = 0$ if the individuals do not touch each other; otherwise, it equals the argument x. Similarly, the third term $\mathbf{f}_{iW}$ denotes a physical contact force induced by body collisions with walls at extreme densities

$$\mathbf{f}_{iW} = kg(r_i - d_{iW})\,\mathbf{n}_{iW} \tag{11}$$

TABLE I
PROBABILITY OF SPECIFIC DECISIONS UNDER VARIOUS EXPERIMENTAL CONDITIONS

Experimental Group	Obstacle Width	Time Pressure	Subgroup Size	Maintaining ($X_g = 0$)			Splitting-merging ($X_g = 1$)		
				Left-side ($Y_g = -1$)	Equal-side ($Y_g = 0$)	Right-side ($Y_g = 1$)	Left-side ($Y_g = -1$)	Equal-side ($Y_g = 0$)	Right-side ($Y_g = 1$)
W1-T1-S1	2 m	$+\infty$ s	2	0.000	0.000	0.917	0.000	0.083	0.000
W1-T1-S2	2 m	$+\infty$ s	3	0.083	0.000	0.917	0.000	0.000	0.000
W1-T1-S3	2 m	$+\infty$ s	4	0.000	0.000	0.917	0.000	0.083	0.000
W1-T2-S1	2 m	8 s	2	0.000	0.000	1.000	0.000	0.000	0.000
W1-T2-S2	2 m	8 s	3	0.000	0.000	1.000	0.000	0.000	0.000
W1-T2-S3	2 m	8 s	4	0.083	0.000	0.667	0.083	0.167	0.000
W1-T3-S1	2 m	5 s	2	0.083	0.000	0.833	0.000	0.083	0.000
W1-T3-S2	2 m	5 s	3	0.000	0.000	0.167	0.167	0.000	0.667
W1-T3-S3	2 m	5 s	4	0.000	0.000	0.000	0.167	0.667	0.167
W2-T1-S1	3 m	$+\infty$ s	2	0.000	0.000	0.917	0.000	0.083	0.000
W2-T1-S2	3 m	$+\infty$ s	3	0.000	0.000	0.500	0.167	0.000	0.333
W2-T1-S3	3 m	$+\infty$ s	4	0.000	0.000	0.583	0.000	0.250	0.167
W2-T2-S1	3 m	8 s	2	0.083	0.000	0.250	0.000	0.667	0.000
W2-T2-S2	3 m	8 s	3	0.000	0.000	0.000	0.083	0.000	0.917
W2-T2-S3	3 m	8 s	4	0.000	0.000	0.083	0.083	0.750	0.083
W2-T3-S1	3 m	5 s	2	0.000	0.000	0.250	0.000	0.750	0.000
W2-T3-S2	3 m	5 s	3	0.000	0.000	0.083	0.250	0.000	0.667
W2-T3-S3	3 m	5 s	4	0.000	0.000	0.000	0.000	0.917	0.083
W3-T1-S1	4 m	$+\infty$ s	2	0.083	0.000	0.833	0.000	0.083	0.000
W3-T1-S2	4 m	$+\infty$ s	3	0.083	0.000	0.417	0.000	0.000	0.500
W3-T1-S3	4 m	$+\infty$ s	4	0.000	0.000	0.000	0.167	0.750	0.083
W3-T2-S1	4 m	8 s	2	0.167	0.000	0.500	0.000	0.333	0.000
W3-T2-S2	4 m	8 s	3	0.000	0.000	0.000	0.333	0.000	0.667
W3-T2-S3	4 m	8 s	4	0.000	0.000	0.000	0.000	1.000	0.000
W3-T3-S1	4 m	5 s	2	0.083	0.000	0.250	0.000	0.667	0.000
W3-T3-S2	4 m	5 s	3	0.000	0.000	0.083	0.250	0.000	0.667
W3-T3-S3	4 m	5 s	4	0.000	0.000	0.000	0.000	0.917	0.083

where d_{iW} is the distance from the center of mass of subgroup member i to wall W, and $\mathbf{n}_{iW}$ stands for the normalized vector perpendicular to it.

D. Parameter Settings of the Proposed Model

As this model is designed to simulate the decision-making and motion behavior of subgroups when facing a static obstacle in a certain scenario, most parameters are therefore given based on our previous experiments and the relevant literature. In terms of decision-making, three control variables (obstacle width, time pressure, and subgroup size) have been experimentally shown to affect the movement states and preferences; thus, the probability $P(Y_g = n \,|X_g = m)$ of subgroup g making a specific decision under each condition is consistent with the experimental results, as shown in Table I. With regard to motion behavior, the maximum horizon distance $d_{\max} = 10\,\mathrm{m}$, pedestrian mass $m_i = 60\,\mathrm{kg}$, pedestrian radius $r_i = 0.2\,\mathrm{m}$, characteristic time $\tau_i = 0.5\,\mathrm{s}$, and body elasticity coefficient $k = 5 \times 10^3\,\mathrm{kg\,s^{-2}}$ are referenced from [34]. For subgroups moving in a splitting-merging state, we observed that members frequently turn their heads to find companions in the merging process after passing through the obstacle, from this the vision angle (half-side) φ is assumed as 180° (i.e., the global field of view), while it is set to 90° (i.e., the front half of the field of view) in other cases. Given that the initial and maximum desired speeds are largely affected by time pressure, we set $v_i^0 \sim \mathcal{N}(1.51, 0.19^2)\,\mathrm{m\,s^{-1}}$ and $v_i^{\max} = 3.98\,\mathrm{m\,s^{-1}}$ in nonemergency situations, $v_i^0 \sim \mathcal{N}(2.15, 0.29^2)\,\mathrm{m\,s^{-1}}$ and $v_i^{\max} = 4.90\,\mathrm{m\,s^{-1}}$ in mild emergency situations, $v_i^0 \sim \mathcal{N}(2.90, 0.23^2)\,\mathrm{m\,s^{-1}}$ and $v_i^{\max} = 5.18\,\mathrm{m\,s^{-1}}$ in severe emergency situations according to experimental data [30].

III. NUMERICAL SIMULATIONS

A. Analysis of the Optimal Region of Model Parameters

The purpose of this section is to optimize two key model parameters by using experimental data and explore how the three control variables (obstacle width, time pressure, and subgroup size) change the optimal domain of model parameters. In this model, as illustrated in Fig. 2, $d_i^{\min}$ and $d_i^{\max}$ are the minimum and maximum critical distances that determine the variation in the follow willingness coefficient α_i. First, the willingness that drives member i to follow other members will not occur if $d_{ic} < d_i^{\min}$, which represents that $d_i^{\min}$ is essentially an indicator that mainly controls the spatial cohesion of subgroups during movement. Second, the willingness that drives member i to follow other members will reach maximum saturation if $d_{ic} > d_i^{\max}$, which implies that $d_i^{\max}$ is an indicator that mainly controls the attraction intensity of subgroups during movement. Because these two model parameters are hard to be reflected

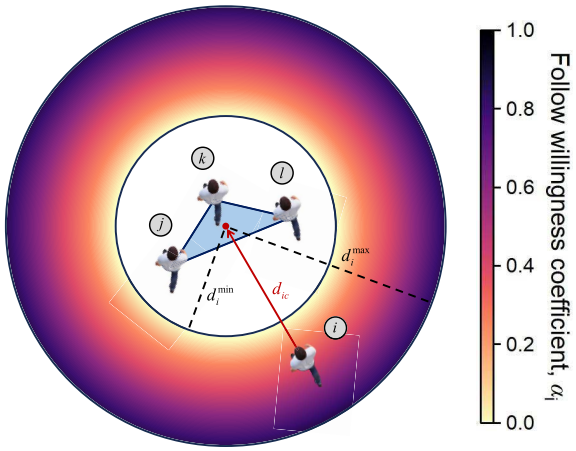

Fig. 2. Illustration of the minimum and maximum critical distances $d_i^{\min}$ and $d_i^{\max}$ that determine the variation in the follow willingness coefficient α_i. A subgroup member i attempts to follow other members j, k, and l within the same subgroup.

intuitively in previous experiments, we compare our model simulations with the experimental results to optimal them for subsequent analysis.

We proportionally scale the experimental scenario to a simulation scenario (i.e., each pixel corresponds to a 0.1 m-side square), and set up 27 simulation groups with exactly the same conditions as the 27 experimental groups by combining different values of the three control variables. Regarding the candidate values of model parameters, the minimum critical distance $d_i^{\min}$ is taken from 0.4 to 1.8 m at intervals of 0.1 m, and the maximum critical distance $d_i^{\max}$ is traversed from 3.0 to 10.0 m at intervals of 0.5 m. Given that some parameter settings (e.g., initial desired speed) related to subgroup members in simulations cannot be fully consistent with real situations in experiments, we therefore repeat the simulation 100 times under each condition and select 12 simulated subgroup trajectories that are closest to 12 experimental subgroup trajectories as effective data. For this, the Hausdorff distance $H(S_i, E_i)$ (i.e., a popular distance metric for shape matching and trajectory analysis) is used to measure the spatial (shape) similarity between simulated trajectory $S_i = \{\mathbf{s}_i^1, \mathbf{s}_i^2, \cdots, \mathbf{s}_i^p\}$ and experimental trajectory $E_i = \{\mathbf{e}_i^1, \mathbf{e}_i^2, \cdots, \mathbf{e}_i^p\}$ of subgroup member i, as given by:

$$H(S_i, E_i) = \max\{h(S_i, E_i), h(E_i, S_i)\} \tag{12}$$

where $h(S_i, E_i) = \max_{\mathbf{s}_i^m \in S_i}\{\min_{\mathbf{e}_i^n \in E_i} \|\mathbf{s}_i^m - \mathbf{e}_i^n\|\}$ is the one-sided Hausdorff distance, whereby the average Hausdorff distance of subgroup g can be expressed as $\langle H(S_i, E_i)\rangle_{i \in g}$.

Fig. 3 shows the average Hausdorff distance between simulated subgroup trajectories and experimental subgroup trajectories under different candidate values of model parameters $d_i^{\min}$ and $d_i^{\max}$. Here, we set up a 3×3 grid as the region of interest (ROI) to calculate the mean value within it and then move it to traverse the entire area. The ROI with the smallest mean value (marked by a red box) is regarded as the optimal region of model parameters (i.e., parameter values in this region make simulation results closest to experimental data). The average Hausdorff distances $[0.5, 0.7\,\text{m}]$ in optimal regions are relatively small, which reflects the effectiveness of our model in reproducing experimental trajectories. From the horizontal direction, the optimal range of $d_i^{\min}$ is always $[0.4, 0.6\,\text{m}]$ regardless of changes in control variables, implying that the spatial cohesion has always been maintained at a high level. This matches well with the setup in previous experiments, in which participants were instructed to move as congregated a form as possible. From the vertical direction, the optimal range of $d_i^{\max}$ is affected to varying degrees by the three control variables. Fig. 3(a)–3(c) shows that $d_i^{\max}$ becomes significantly larger if the obstacle width is expanded because members will retain lower attraction intensity to avoid excessive sharp turns due to longer lateral distances required to move in the merging process. $d_i^{\max}$ keeps at a higher level in emergency situations compared to that in nonemergency situations, as shown in Fig. 3(d)–3(f), since members are more willing to reach the terminal line with a shorter path than merging with other members. As the subgroup size increases in Fig. 3(g)–3(i), the sequential decrease of $d_i^{\max}$ indicates that the attraction intensity is growing, this may result from larger subgroups having a stronger sense of identity. Overall, these results essentially reflect the variations in spatial cohesion and attraction intensity of subgroups under the three control variables, which is beneficial in providing reasonable parameter settings for different simulation conditions.

B. Effect of the Spatial Cohesion on the Movement Process

Our goal here is to investigate how the spatial cohesion of subgroups affects the movement process. First, we control the maximum critical distance as $d_i^{\max} = 6.5\,\text{m}$ and then set up two cases of high ($d_i^{\min} = 0.6\,\text{m}$) and low ($d_i^{\min} = 1.6\,\text{m}$) spatial cohesion as examples. Fig. 4 displays the snapshots of the movement process of subgroups with different spatial cohesion in the two movement states. The movement pattern of subgroups after passing through the obstacle is strongly dependent on spatial cohesion, whereas that before passing through the obstacle is almost independent of it. If the subgroup moves in a maintaining state, as shown in Fig. 4(a) and 4(b), members with high spatial cohesion are close to each other, otherwise they will keep larger relative distances to arrive at the terminal line. If the subgroup moves in a splitting-merging state, Fig. 4(c) and 4(d) indicates that members with high spatial cohesion merge faster and reach the terminal line together, but conversely it is hard for them to gather near the terminal line and their position distribution is relatively loose. This preliminarily provides a qualitative description for the role of spatial cohesion when subgroups pass through the obstacle.

To quantitatively analyze the impact of the spatial cohesion on physical quantities during movement, we simulate each of the two movement states in 27 simulation groups 100 times under different candidate values of model parameters $d_i^{\min}$ and $d_i^{\max}$ and calculate the overall average at each candidate value of $d_i^{\min}$. The first physical quantity is distance, which is

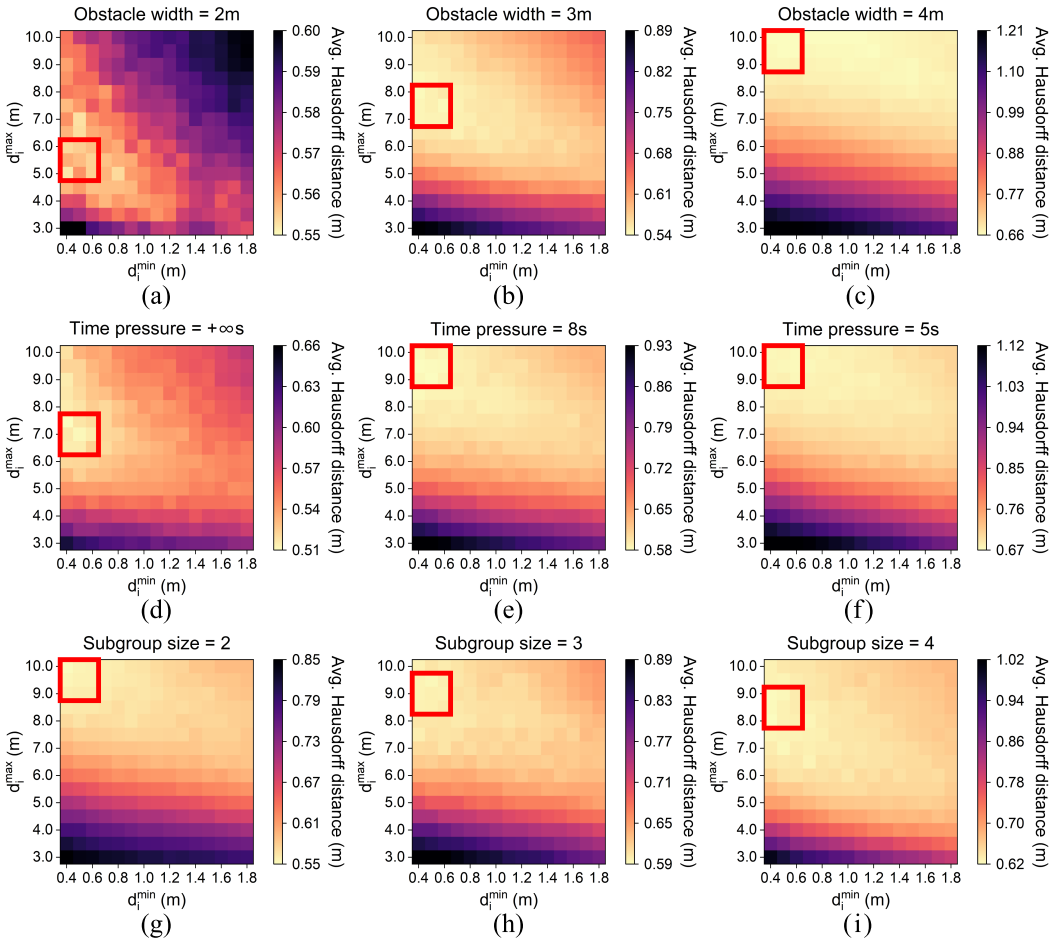

Fig. 3. Average Hausdorff distance between simulated subgroup trajectories and experimental subgroup trajectories under different candidate values of model parameters $d_i^{\min}$ and $d_i^{\max}$. (a)–(c) Obstacle width $=$ 2, 3, 4 m. (d)–(f) Time pressure $= +\infty$, 8, 5 s. (g)–(i) Subgroup size $=$ 2, 3, 4.

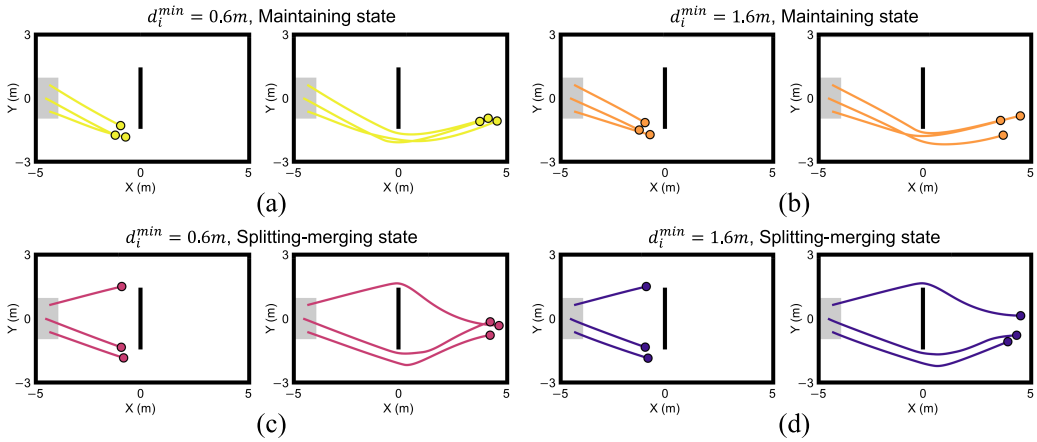

Fig. 4. Snapshots of the movement process of subgroups with different spatial cohesion in the two movement states. (a) $d_i^{\min} = 0.6$ m, maintaining state. (b) $d_i^{\min} = 1.6$ m, maintaining state. (c) $d_i^{\min} = 0.6$ m, splitting-merging state. (d) $d_i^{\min} = 1.6$ m, splitting-merging state.

specified as the path length of subgroup members from leaving the initial area to reaching the terminal line. Fig. 5 shows the path length as a function of $d_i^{\min}$ in the two movement states under different control variables. It can be observed that the obstacle width has the most significant effect on path length, which manifests in the fact that members should detour for longer distances to pass through a wider obstacle. Both urgent time pressure in the two movement states and large

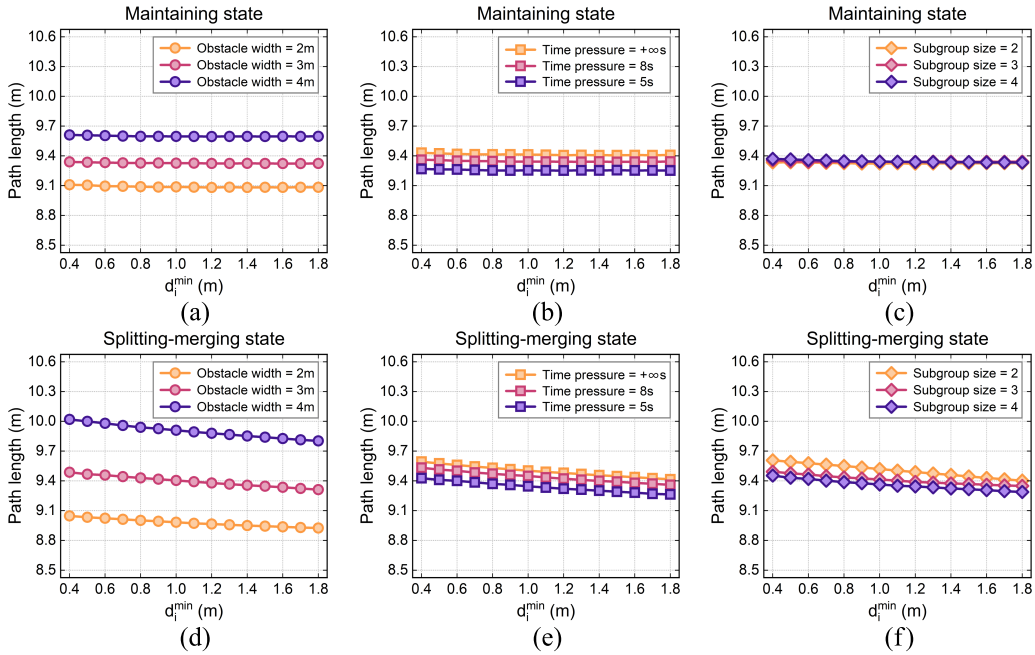

Fig. 5. Path length as a function of $d_i^{\min}$ in the two movement states under different control variables. (a) Maintaining state, obstacle width $=$ 2, 3, 4 m. (b) Maintaining state, time pressure $=$ $+\infty$, 8, 5 s. (c) Maintaining state, subgroup size $=$ 2, 3, 4. (d) Splitting-merging state, obstacle width $=$ 2, 3, 4 m. (e) Splitting-merging state, time pressure $=$ $+\infty$, 8, 5 s. (f) Splitting-merging state, subgroup size $=$ 2, 3, 4.

subgroup size in the splitting-merging state will slightly shorten the path length. The subgroup moving in a maintaining state tends to keep a relatively fixed organizational structure, whereby the spatial cohesion has no obvious impact on path length. However, the path length becomes near-linear shorter as the spatial cohesion weakens ($d_i^{\min}$ increases) if the subgroup moves in a splitting-merging state, because the reduced willingness to merge with other members will decrease additional displacements triggered by advance merging behavior.

The other physical quantity is time, which is defined as the movement time of subgroup members from leaving the initial area to reaching the terminal line. The movement time as a function of $d_i^{\min}$ in the two movement states under different control variables is presented in Fig. 6. By analyzing the impact of the three control variables, we find that an enlarged obstacle width slightly increases the movement time, a more urgent time pressure makes the movement time significantly shorter, but the variation in subgroup size does not substantially change the movement time. Interestingly, regardless of movement state, the spatial cohesion of subgroups has almost no significant influence on movement time, perhaps this is balanced by other factors such as the adjustment in movement speed. In summary, the spatial cohesion has a relatively small effect on the movement process, which only significantly alters the path length in the splitting-merging state but not in the maintaining state and barely impacts the movement time in both movement states.

C. *Effect of the Attraction Intensity on the Movement Process*

Turning now to the effect of the attraction intensity on the movement process. We similarly fix the minimum critical distance to $d_i^{\min} = 1.1$ m and then adjust another model parameter to set up two cases of high ($d_i^{\max} = 4.0$ m) and low ($d_i^{\max} = 9.0$ m) attraction intensities. The snapshots of the movement process of subgroups with different attraction intensities in the two movement states are illustrated in Fig. 7. For the maintaining state in Fig. 7(a) and 7(b), the difference in attraction intensity has almost no effect on the movement process, which might be that the distances from subgroup members to the centroid always remain below the minimum critical distance $d_i^{\min}$. For the splitting-merging state in Fig. 7(c) and 7(d), the movement pattern of subgroups before passing through the obstacle is also independent of the attraction intensity, but members with high attraction intensity quickly congregate together to reach the terminal line after passing through it. This is because the willingness to merge with other members is more dominant than taking a shorter path to the terminal line. These results basically reveal that the role of attraction intensity may differ across varying situations.

Based on simulation results in the previous section, we also take the overall average at each candidate value of $d_i^{\max}$ to analyze the impact of the attraction intensity on physical quantities during movement. Fig. 8 shows the path length as a function of $d_i^{\max}$ under different control variables, which presents obvious differences in the two movement states. If the subgroup moves in a maintaining state, the path length

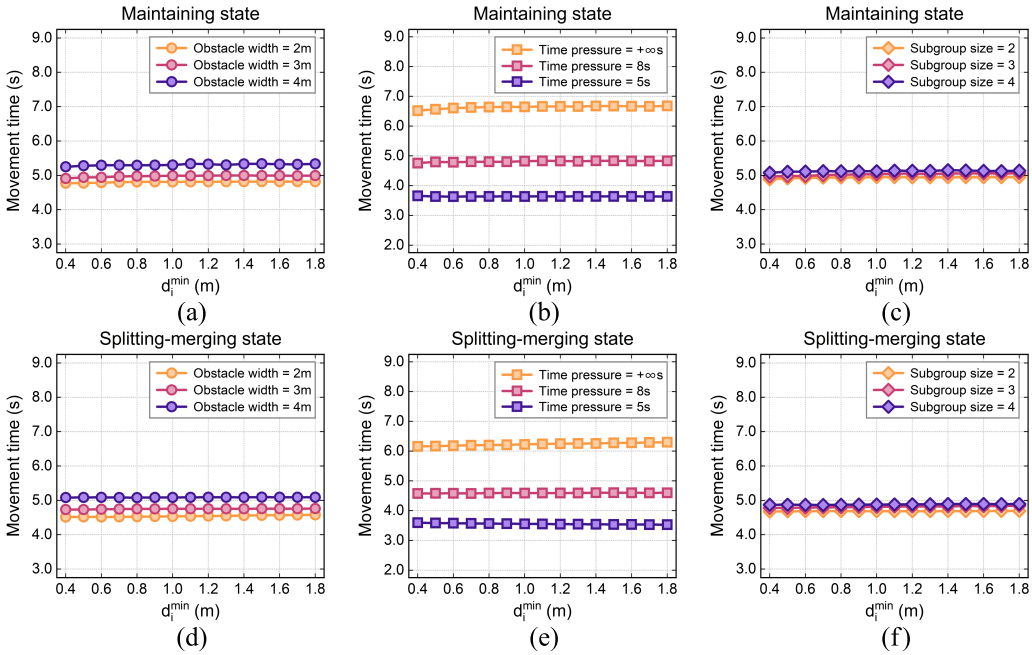

Fig. 6. Movement time as a function of $d_i^{\min}$ in the two movement states under different control variables. (a) Maintaining state, obstacle width $=$ 2, 3, 4 m. (b) Maintaining state, time pressure $=+\infty$, 8, 5 s. (c) Maintaining state, subgroup size $=$ 2, 3, 4. (d) Splitting-merging state, obstacle width $=$ 2, 3, 4 m. (e) Splitting-merging state, time pressure $=+\infty$, 8, 5 s. (f) Splitting-merging state, subgroup size $=$ 2, 3, 4.

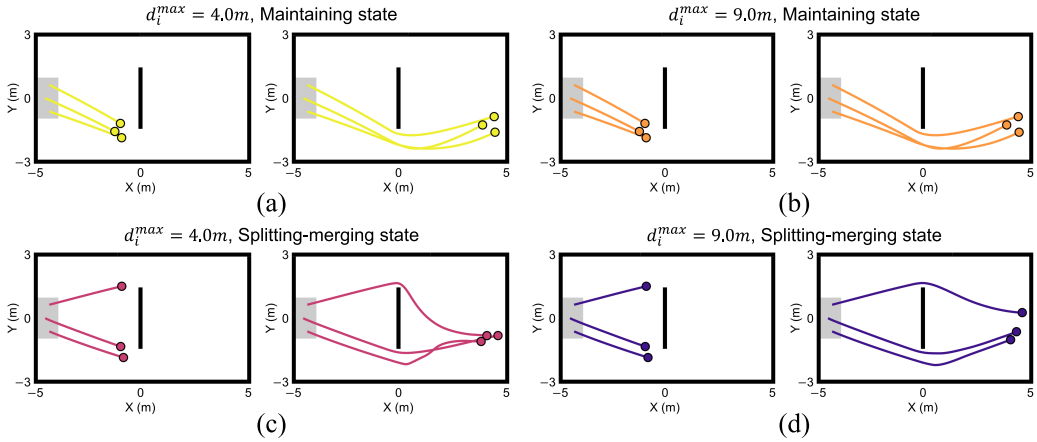

Fig. 7. Snapshots of the movement process of subgroups with different attraction intensities in the two movement states. (a) $d_i^{\max} = 4.0$ m, maintaining state. (b) $d_i^{\max} = 9.0$ m, maintaining state. (c) $d_i^{\max} = 4.0$ m, splitting-merging state. (d) $d_i^{\max} = 9.0$ m, splitting-merging state.

remains almost constant as the attraction intensity changes. As members have formed a relatively stable organizational structure when they move together, no additional attraction is necessary to avoid separation in most cases. If the subgroup moves in a splitting-merging state, the path length decreases nonlinearly as the attraction intensity reduces ($d_i^{\max}$ increases) and finally reaches a near-saturation state. In other words, the merging process of subgroup members gradually changes from "first merge quickly and then reach the terminal line together" to "move with a more direct path to merge near the terminal line." This is essentially analogous to the fact that as the two short sides of a triangle converge to the third long side, the sum of their lengths shows a nonlinear decreasing trend.

This part concerns the impact of the attraction intensity on movement time, and the functional relationship corresponding to the two movement states under different control variables is shown in Fig. 9. It can be seen from Fig. 9(a)–9(c) that the variation in attraction intensity also does not change the movement time in the maintaining state, the reason is consistent with the previously mentioned one that it is basically independent of the attraction intensity if the subgroup moves with a relatively

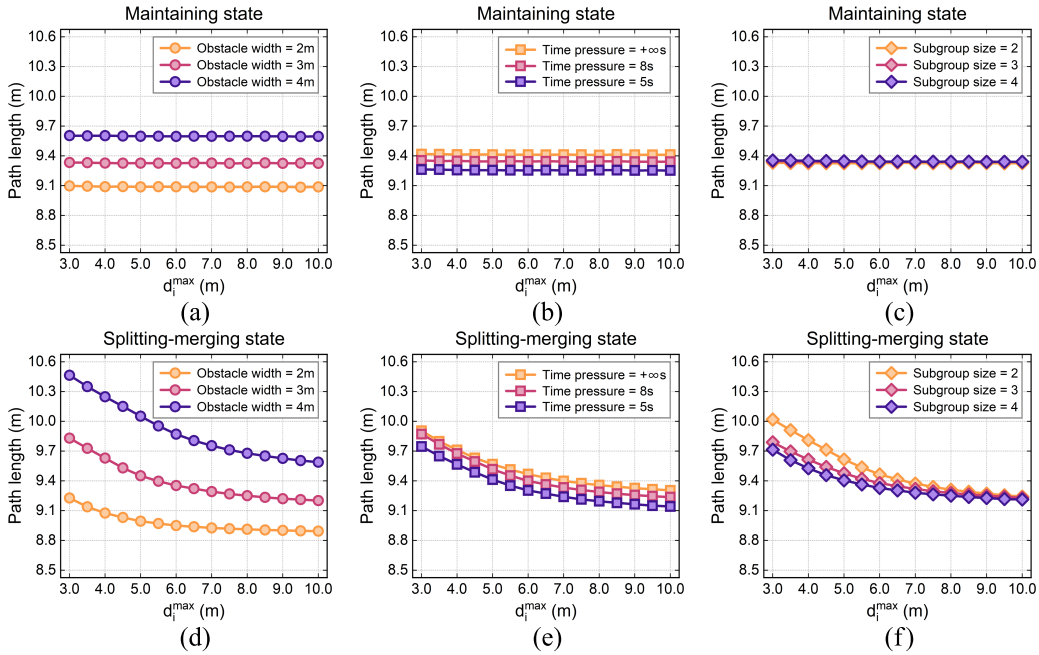

Fig. 8. Path length as a function of $d_i^{\max}$ in the two movement states under different control variables. (a) Maintaining state, obstacle width $=$ 2, 3, 4 m. (b) Maintaining state, time pressure $=$ $+\infty$, 8, 5 s. (c) Maintaining state, subgroup size $=$ 2, 3, 4. (d) Splitting-merging state, obstacle width $=$ 2, 3, 4 m. (e) Splitting-merging state, time pressure $=$ $+\infty$, 8, 5 s. (f) Splitting-merging state, subgroup size $=$ 2, 3, 4.

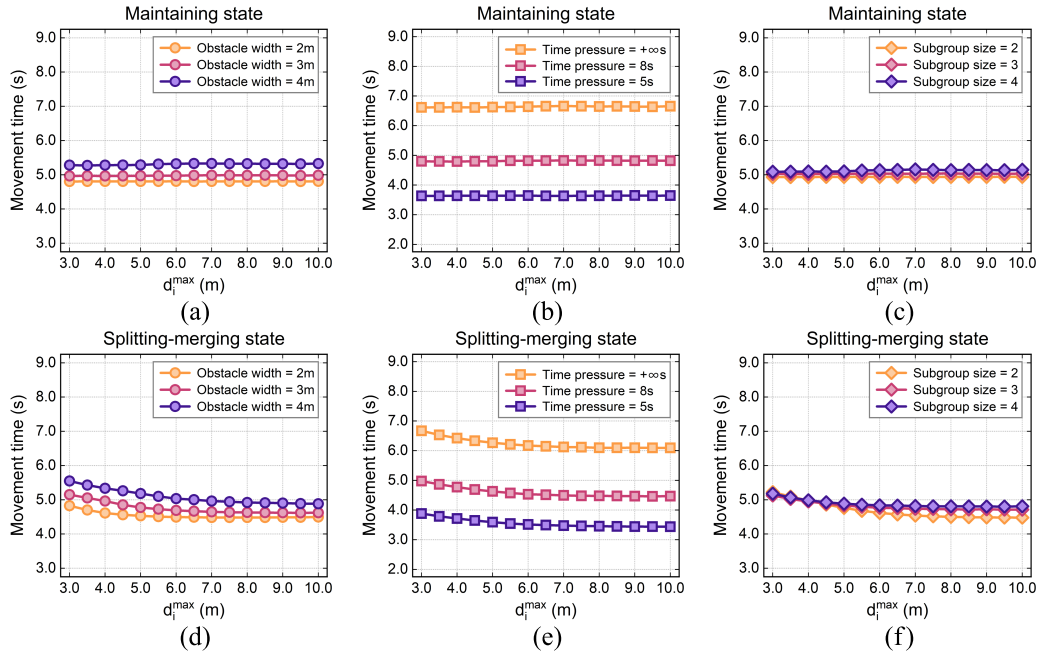

Fig. 9. Movement time as a function of $d_i^{\max}$ in the two movement states under different control variables. (a) Maintaining state, obstacle width $=$ 2, 3, 4 m. (b) Maintaining state, time pressure $=$ $+\infty$, 8, 5 s. (c) Maintaining state, subgroup size $=$ 2, 3, 4. (d) Splitting-merging state, obstacle width $=$ 2, 3, 4 m. (e) Splitting-merging state, time pressure $=$ $+\infty$, 8, 5 s. (f) Splitting-merging state, subgroup size $=$ 2, 3, 4.

stable organizational structure. For the splitting-merging state in Fig. 9(d)–9(f), a slight decrease and eventual saturation of the movement time can be observed as $d_i^{\max}$ becomes larger. This indicates that although a higher attraction intensity can promote the merging speed of subgroup members, it actually induces longer delays in the overall process, which may be caused by extra path length and coordination time during aggregation. As a result, the variability in attraction intensity hardly changes

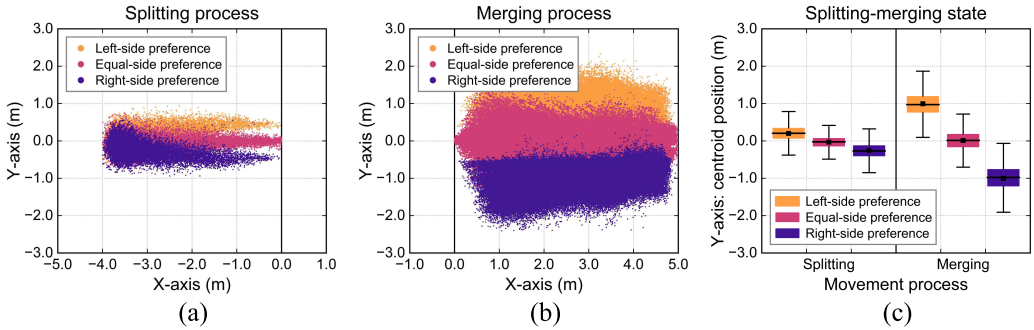

Fig. 10. Analysis of the splitting and merging processes under different movement preferences. (a) and (b) Centroid positions at the start of the splitting process and at the end of the merging process. (c) Boxplots of the centroid positions projected on the Y-axis.

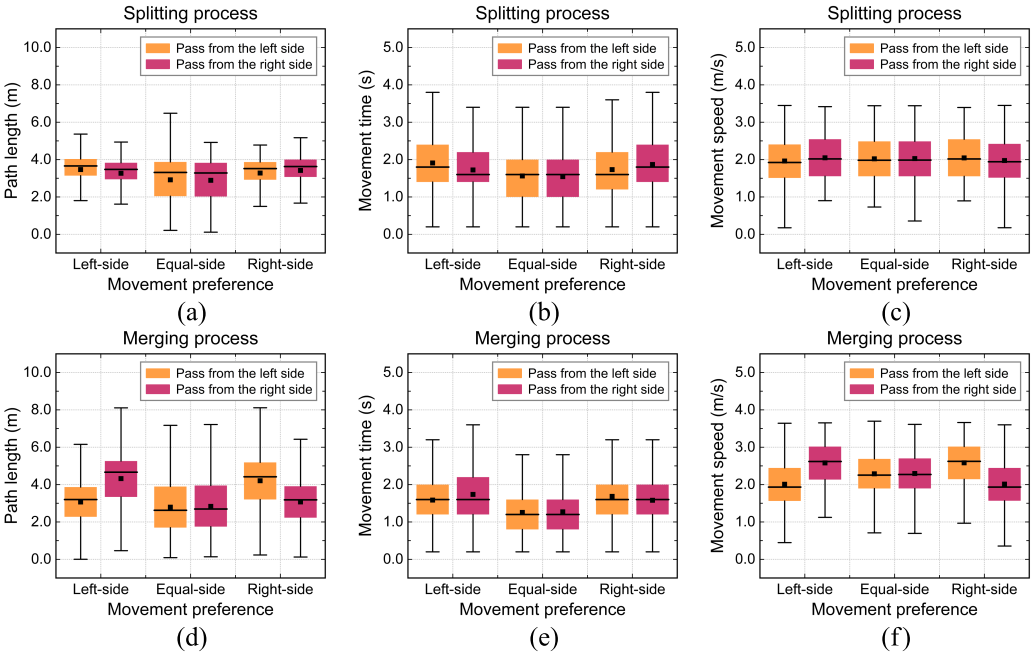

Fig. 11. Statistical analysis on physical quantities for subgroup members passing from the left and right sides of the obstacle in the splitting and merging processes under different movement preferences. (a)–(c) Path length, movement time, and movement speed in the splitting process. (d)–(f) Path length, movement time, and movement speed in the merging process.

the movement process in the maintaining state but significantly dominates path length and movement time in the splitting-merging state.

D. Validation of the Herding Effect in the Merging Process

In this section, we are interested in simulating the splitting-merging state of subgroups as this has received little attention in existing models. According to relevant definitions: the splitting process represents that subgroup members separate from a congregated form and move to both sides of the obstacle, and the merging process means that subgroup members move from both sides of the obstacle to reorganize into a congregated form [30]. Here, the congregated form is approximately defined as the distances from subgroup members to the centroid do not exceed the minimum critical distance $d_i^{\min}$. For the splitting and merging processes in Fig. 10(a) and 10(b), the arrangement order of centroid positions along the Y-axis direction basically corresponds to the movement preference. Fig. 10(c) further shows that the difference in centroid positions projected on the Y-axis at the end of the merging process is significantly larger than that at the start of the splitting process, indicating that there may be certain effects to shift the congregated point laterally in the merging process. The above results are quite consistent with the findings in previous experiments [30], which reflect the effectiveness of our model in reproducing the splitting and merging processes of subgroups.

Fig. 11 presents the statistical analysis on physical quantities for subgroup members passing from the left and right sides of the obstacle in the splitting and merging processes under different movement preferences. For subgroups with an equal-side preference, there is almost no obvious difference in path

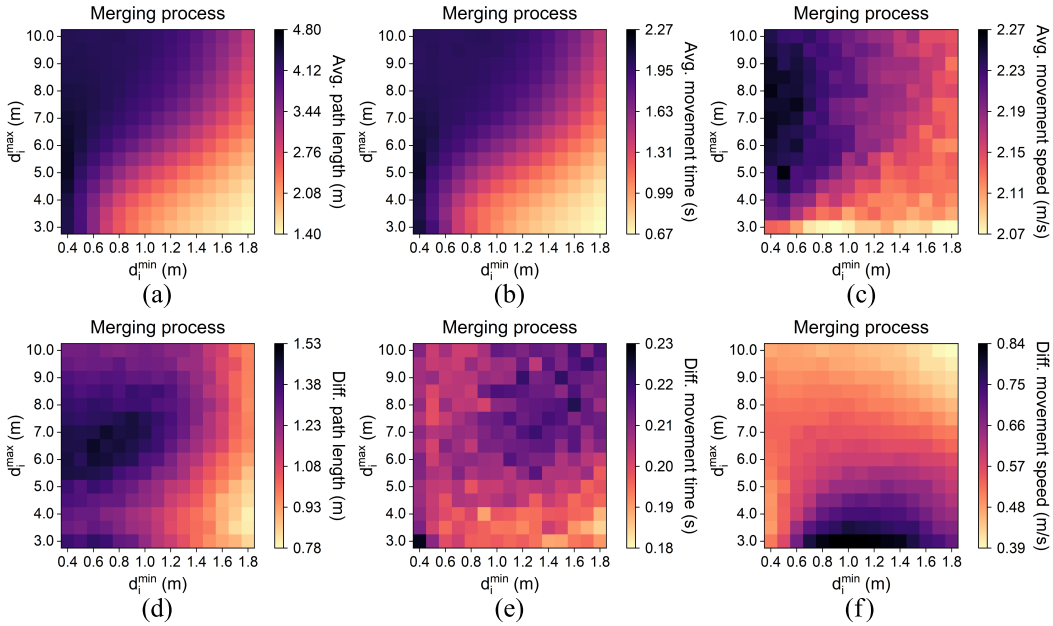

Fig. 12. Statistical analysis on physical quantities for subgroup members passing from the left and right sides of the obstacle in the merging process under different candidate values of model parameters $d_i^{\min}$ and $d_i^{\max}$. (a)–(c) Average value of path length, movement time, and movement speed. (d)–(f) Absolute difference of path length, movement time, and movement speed.

length, movement time, and movement speed between members passing from both sides due to the symmetry principle. For subgroups with a left(right)-side preference in the splitting process, as shown in Fig. 11(a)–11(c), members who pass from the left(right)-side have slightly longer path lengths and movement times but relatively lower movement speeds than those who pass from the right(left)-side. Because there is a probability of congestion on the side with more members passing through the obstacle, which will trigger the detouring behavior and forced deceleration of some members. For subgroups with a left(right)-side preference in the merging process, as shown in Fig. 11(d)–11(f), we find that the movement time is almost the same, and the part with fewer members passing from one side significantly requires longer path lengths and faster movement speeds to approach the part with more members passing from another side. This further validates that our model can simulate the herding effect of subgroup members in the merging process.

In the final part, we want to know the effect of two key model parameters on the herding effect in the merging process. Under different candidate values of model parameters $d_i^{\min}$ and $d_i^{\max}$, Fig. 12(a)–12(c) illustrate the average value of physical quantities for members passing from the left and right sides of the obstacle. The increase of $d_i^{\min}$ and decrease of $d_i^{\max}$ lead to a consistent shortening of the average path length and average movement time, while the average movement speed varies little under the modulation of model parameters. This suggests that the spatial cohesion and attraction intensity directly affect the path length moving from both sides of the obstacle to the congregated form, thereby indirectly adjusting the time consumed by the merging process. Similarly, the absolute difference of physical quantities for members passing from the left and right sides of the obstacle is exhibited in Fig. 12(d)–12(f). It is notable that the difference in path length is greatest at high spatial cohesion and medium attraction intensity, but the greatest difference in movement speed occurs at medium spatial cohesion and high attraction intensity. This reveals the potential regions of model parameters that may give rise to the most significant herding effect in the merging process. Besides, the difference in movement time is not evident since the merging process is terminated simultaneously, with only a slight variation in the onset time.

IV. Conclusion

In this article, we propose a vision-driven model in which the characteristic laws of the decision-making and motion behavior of subgroups in previous experiments are mathematically integrated. This model simulates the coordinated movement of subgroups when facing a static obstacle by controlling spatial cohesion and attraction intensity. Numerical simulations show that the optimal regions of model parameters vary under different conditions of the three control variables (obstacle width, time pressure, and subgroup size). The spatial cohesion and attraction intensity mainly affect the movement process of subgroups in the splitting-merging state, where the weakening of spatial cohesion makes the path length near-linear shorter, and the decreasing attraction intensity leads to a nonlinear reduction of path length and movement time. Our model can effectively reproduce the herding effect of subgroup members in the merging process, which is also affected to varying degrees by the modulation of model parameters.

This work can be regarded as a vital supplement to our previous experimental study and may provide implications for potential application areas. For crowd evacuation, the

movement process of subgroups interacting with obstacles can be simulated by the proposed model, and this may help formulate more effective evacuation strategies and reduce crowd disasters [11]. In terms of architectural design, one can adopt this model to characterize subgroup behaviors in scenarios with various obstacle layouts, which is beneficial to maximize the optimization of crowd mobility and space utilization [35]. Regarding swarm robotics, our model can inspire the development of distributed perception and decision-making algorithms, which allows swarm robotics to adaptively adjust motion strategies when facing obstacles and improve collaborative ability in complex environments [36].

This model allows us to use simulations to further explore the effects of certain variables that are hard to control in experiments, but a possible limitation is the strong dependence on specific experimental scenarios and data. This somewhat weakens model scalability and transferability because environmental layouts (e.g., terrain and obstacle type) and personal attributes (e.g., body shape and desired speed) are various in reality. Thus, we expect that future research can obtain more extensive data and laws on the interactions between subgroups with obstacles via diverse experimental settings, which will help produce general models to simulate subgroup behaviors more realistically. Moreover, recent advancements in human pose estimation could potentially be applied to analyze the movement process of subgroups and offer new insight into the behavioral patterns of individuals within a subgroup [37]. In conclusion, this work facilitates our understanding of subgroup behaviors from a sociopsychological perspective [38].

REFERENCES

[1] V. J. Kok, M. K. Lim, and C. S. Chan, "Crowd behavior analysis: A review where physics meets biology," *Neurocomputing*, vol. 177, pp. 342–362, Feb. 2016.

[2] M. Bendali-Braham, J. Weber, G. Forestier, L. Idoumghar, and P.-A. Muller, "Recent trends in crowd analysis: A review," *Mach. Learn. Appl.*, vol. 4, Jun. 2021, Art. no. 100023.

[3] P. Kothari, S. Kreiss, and A. Alahi, "Human trajectory forecasting in crowds: A deep learning perspective," *IEEE Trans. Intell. Transp. Syst.*, vol. 23, no. 7, pp. 7386–7400, Jul. 2022.

[4] J. Fu et al., "Dual attention network for scene segmentation," in *Proc. IEEE/CVF Conf. Comput. Vis. Pattern Recognit. (CVPR),* Piscataway, NJ, USA: IEEE Press, Jun. 2019, pp. 3146–3154.

[5] J. Gao, T. Han, Y. Yuan, and Q. Wang, "Domain-adaptive crowd counting via high-quality image translation and density reconstruction," *IEEE Trans. Neural Netw. Learn. Syst.*, vol. 34, no. 8, pp. 4803–4815, Aug. 2023.

[6] G. Batchuluun, J. H. Kim, H. G. Hong, J. K. Kang, and K. R. Park, "Fuzzy system based human behavior recognition by combining behavior prediction and recognition," *Expert Syst. Appl.*, vol. 81, pp. 108–133, Sep. 2017.

[7] O. P. Popoola and K. Wang, "Video-based abnormal human behavior recognition—A review," *IEEE Trans. Syst., Man, Cybern., Part C (Appl. Rev.)*, vol. 42, no. 6, pp. 865–878, Nov. 2012.

[8] D. Helbing, L. Buzna, A. Johansson, and T. Werner, "Self-organized pedestrian crowd dynamics: Experiments, simulations, and design solutions," *Transp. Sci.*, vol. 39, no. 1, pp. 1–24, Feb. 2005.

[9] D. Sharma, A. P. Bhondekar, A. K. Shukla, and C. Ghanshyam, "A review on technological advancements in crowd management," *J. Ambient Intell. Humanized Comput.*, vol. 9, no. 3, pp. 485–495, Nov. 2016.

[10] A. Nicolas and F. H. Hassan, "Social groups in pedestrian crowds: Review of their influence on the dynamics and their modelling," *Transportmetrica A: Transport Sci.*, vol. 19, no. 1, Jan. 2023, Art. no. 1970651.

[11] W. Wu and X. Zheng, "A systematic analysis of subgroup research in pedestrian and evacuation dynamics," *IEEE Trans. Intell. Transp. Syst.*, vol. 25, no. 2, pp. 1225–1246, Feb. 2024.

[12] W. Wu, W. Yi, X. Wang, and X. Zheng, "A force-based model for adaptively controlling the spatial configuration of pedestrian subgroups at non-extreme densities," *Transp. Res. Part C: Emerg. Technol.*, vol. 152, Jul. 2023, Art. no. 104154.

[13] M. Moussaïd, N. Perozo, S. Garnier, D. Helbing, and G. Theraulaz, "The walking behaviour of pedestrian social groups and its impact on crowd dynamics," *PLoS One*, vol. 5, no. 4, Apr. 2010, Art. no. e10047.

[14] F. Zanlungo, T. Ikeda, and T. Kanda, "Potential for the dynamics of pedestrians in a socially interacting group," *Phys. Rev. E*, vol. 89, no. 1, Jan. 2014, Art. no. 012811.

[15] Y. Hu, J. Zhang, W. Song, and N. W. Bode, "Social groups barely change the speed-density relationship in unidirectional pedestrian flow, but affect operational behaviours," *Saf. Sci.*, vol. 139, Jul. 2021, Art. no. 105259.

[16] R. Ye et al., "Traffic dynamics of uni- and bidirectional pedestrian flows including dyad social groups in a ring-shaped corridor," *J. Statist. Mechan. Theory Experiment*, vol. 2021, no. 2, Feb. 2021, Art. no. 023406.

[17] C. von Krüchten and A. Schadschneider, "Empirical study on social groups in pedestrian evacuation dynamics," *Physica A: Statist. Mechan. Appl.*, vol. 475, pp. 129–141, Jun. 2017.

[18] M. Haghani, M. Sarvi, Z. Shahhoseini, and M. Boltes, "Dynamics of social groups' decision-making in evacuations," *Transp. Res. Part C: Emerg. Technol.*, vol. 104, pp. 135–157, Jul. 2019.

[19] C. Zhou, M. Han, Q. Liang, Y.-F. Hu, and S.-G. Kuai, "A social interaction field model accurately identifies static and dynamic social groupings," *Nature Human Behav.*, vol. 3, no. 8, pp. 847–855, Jun. 2019.

[20] L. Huang et al., "Social force model-based group behavior simulation in virtual geographic environments," *ISPRS Int. J. Geo-Inf.*, vol. 7, no. 2, Feb. 2018, Art. no. 79.

[21] D. Helbing, I. Farkas, and T. Vicsek, "Simulating dynamical features of escape panic," *Nature*, vol. 407, no. 6803, pp. 487–490, Sep. 2000.

[22] C. Burstedde, K. Klauck, A. Schadschneider, and J. Zittartz, "Simulation of pedestrian dynamics using a two-dimensional cellular automaton," *Phys. A: Statist. Mechan. Appl.*, vol. 295, nos. 3–4, pp. 507–525, Jun. 2001.

[23] E. Bonabeau, "Agent-based modeling: Methods and techniques for simulating human systems," *Proc. Nat. Acad. Sci.*, vol. 99, pp. 7280–7287, May 2002.

[24] W. Xie, E. W. M. Lee, T. Li, M. Shi, R. Cao, and Y. Zhang, "A study of group effects in pedestrian crowd evacuation: Experiments, modelling and simulation," *Saf. Sci.*, vol. 133, Jan. 2021, Art. no. 105029.

[25] Y. Turgut and C. E. Bozdag, "Modeling pedestrian group behavior in crowd evacuations," *Fire Mater.*, vol. 46, no. 2, pp. 420–442, Apr. 2021.

[26] L. Lu, C.-Y. Chan, J. Wang, and W. Wang, "A study of pedestrian group behaviors in crowd evacuation based on an extended floor field cellular automaton model," *Transp. Res. Part C: Emerg. Technol.*, vol. 81, pp. 317–329, Aug. 2017.

[27] Z. Pan, Q. Wei, and H. Wang, "Agent-based simulation of hindering effect of small group behavior on elevated interval evacuation time along urban rail transit," *Travel Behav. Soc.*, vol. 22, pp. 262–273, Jan. 2021.

[28] N. Shiwakoti, X. Shi, and Z. Ye, "A review on the performance of an obstacle near an exit on pedestrian crowd evacuation," *Saf. Sci.*, vol. 113, pp. 54–67, Mar. 2019.

[29] O. Severiukhina, D. Voloshin, M. Lees, and V. Karbovskii, "The study of the influence of obstacles on crowd dynamics," *Procedia Comput. Sci.*, vol. 108, pp. 215–224, Jun. 2017.

[30] W. Wu, W. Yi, X. Wang, E. Wang, and X. Zheng, "Experimental study on the decision-making and motion behavior of subgroups when facing a static obstacle during movement," *Expert Syst. Appl.*, vol. 242, May 2024, Art. no. 122761.

[31] F. Zanlungo, Z. Yücel, D. Brščić, T. Kanda, and N. Hagita, "Intrinsic group behaviour: Dependence of pedestrian dyad dynamics on principal social and personal features," *PLoS One*, vol. 12, no. 11, Nov. 2017, Art. no. e0187253.

[32] F. Zanlungo, Z. Yücel, and T. Kanda, "Intrinsic group behaviour II: On the dependence of triad spatial dynamics on social and personal features; and on the effect of social interaction on small group dynamics," *PLoS One*, vol. 14, no. 12, Dec. 2019, Art. no. e0225704.

[33] W. Wu, W. Yi, X. Wang, and X. Zheng, "A vision-driven model based on cognitive heuristics for simulating subgroup behaviors during

evacuation," *IEEE Trans. Intell. Transp. Syst.*, vol. 25, no. 11, pp. 16048–16058, Nov. 2024.

[34] M. Moussaïd, D. Helbing, and G. Theraulaz, "How simple rules determine pedestrian behavior and crowd disasters," *Proc. Nat. Acad. Sci.*, vol. 108, no. 17, pp. 6884–6888, Apr. 2011.

[35] M. Haghani, "Optimising crowd evacuations: Mathematical, architectural and behavioural approaches," *Saf. Sci.*, vol. 128, Aug. 2020, Art. no. 104745.

[36] M. Dorigo, G. Theraulaz, and V. Trianni, "Swarm robotics: Past, present, and future [point of view]," *Proc. IEEE*, vol. 109, no. 7, pp. 1152–1165, Jul. 2021.

[37] T. Zhang, Q. Li, J. Wen, and C. Philip Chen, "Enhancement and optimisation of human pose estimation with multi-scale spatial attention and adversarial data augmentation," *Inf. Fusion*, vol. 111, Nov. 2024, Art. no. 102522.

[38] A. Templeton, J. Drury, and A. Philippides, "From mindless masses to small groups: Conceptualizing collective behavior in crowd modeling," *Rev. General Psychol.*, vol. 19, no. 3, pp. 215–229, Sep. 2015.

Wenhan Wu received the B.S. degree in control science and engineering from the School of Automation, Central South University, Changsha, China, in 2019. He is currently working toward the Ph.D. degree in control science and engineering with the Department of Automation, Tsinghua University, Beijing, China. From 2023 to 2024, he was a joint Ph.D. Student with the Institute for Theoretical Biology, Department of Biology, Humboldt Universität zu Berlin, Berlin, Germany.

His research interests include collective behavior, emergency evacuation, pedestrian group, network science, and decision making.

Wenfeng Yi received the B.S. degree in control science and engineering from the School of Astronautics, Beihang University, Beijing, China, in 2019. He is currently working toward the Ph.D. degree in control science and engineering with the Department of Automation, Tsinghua University, Beijing. From 2023 to 2024, he was a joint Ph.D. Student with the School of Biological Sciences, University of Bristol, Bristol, U.K.

His research interests include collective behavior, emergency evacuation, pedestrian queueing, and swarm robotics.

Erhui Wang received the Ph.D. degree in power engineering and engineering thermophysics from the School of Energy and Environmental Engineering, University of Science and Technology Beijing, Beijing, China, in 2023.

He is currently a Postdoctoral Research Fellow with the Department of Automation, Tsinghua University, Beijing. His research interests include partial differential equations, machine learning, swarm intelligence computing, and applied mathematics and modeling.

Xiaolu Wang received the Ph.D. degree in control theory and control engineering from Beijing University of Chemical Technology, Beijing, China, in 2015.

She is currently an Assistant Researcher with the Department of Automation, Tsinghua University, Beijing. Her research interests include crowd evacuation intervention mechanism, evacuation dynamics, and emergency management.

Xiaoping Zheng received the B.S. degree in Chinese materia medica from Traditional Chinese Medicine, Chengdu, China, in 1995, and the Ph.D. degree in political economics from Sichuan University, Chengdu, China, in 2003.

He is currently a Professor with the Department of Automation, Tsinghua University, Beijing, China. From 2004 to 2006, he was a Postdoctoral Researcher with the School of Management, Fudan University, Shanghai, China. From 2006 to 2013, he was a Professor with the Institute of Safety Management, Beijing University of Chemical Technology, Beijing. His research interests include large-scale crowd evacuation, evolutionary game theory, and terahertz technology.

Prof. Zheng was a 973 Chief Scientist in 2011, a recipient of the National Science Fund for Distinguished Young Scholars in 2012, and a Distinguished Professor of the Chang Jiang Scholars Program in 2021.